ACS OMEGA

Open Access

http://pubs.acs.org/journal/acsodf

Article

Selective Inhibitor Design against Thymidylate Synthase of *Mycobacterium tuberculosis* Using Alchemical Simulations

Pallav Sengupta and Priyadarshi Satpati*

Cite This: *ACS Omega* 2025, 10, 13966−13976

Read Online

ACCESS | Metrics & More | Article Recommendations | Supporting Information

ABSTRACT: Thymidylate synthase is an essential enzyme that catalyzes the conversion of deoxyuridine monophosphate (dUMP) to deoxythymidine monophosphate (dTMP). Thymidylate synthase from *Mycobacterium tuberculosis*(MtbThyX) recognizes the deprotonated substrate dUMP$^{(d)}$ (ionized at N3, charge = −3) involving the cationic side chain of Arg199, whereas the human analogue (hThyA) selects the natural substrate dUMP (charge = −2) by involving the polar side chain of Asn226 in the binding pocket. Distinctly different protonation states of the substrate and the catalytic pocket architecture make MtbThyX an attractive drug target for combating *Mycobacterium tuberculosis*. Fluorodeoxyuridylate (FdUMP) is a known inhibitor of thymidylate synthase, which is severely limited by poor selectivity (it is more potent against hThyA relative to MtbThyX). Using FdUMP as a template, we designed three drug-like ligands, L1, L2, and L3, by (1) removing the proton from the Watson−Crick edge and (2) substituting the ketone/hydroxyl group with fluorine and/or a carboxylic moiety. The absence of a proton on the N3 atom of the ligand is intended to ensure selectivity by favoring MtbThyX binding (skipping the N3 ionization requirement) but penalizing hThyA binding (disrupting the interaction with Asn226). Ionization of the carboxyl group in the ligands was expected to increase the affinity in the cationic binding pocket of MtbThyX. Alchemical simulations confirmed that the designed ligands are strongly favored and disfavored relative to the substrate (dUMP) by MtbThyX and hThyA, respectively. In contrast to hThyA, the catalytic pocket of MtbThyX proved to be relatively dry and stabilized the relatively compact conformation of the ligand (which had a noticeable effect on sugar puckering). Favorable protein−ligand electrostatic interactions in the dry MtbThyX pocket strongly favored ligand binding. In contrast, the interaction between the Watson−Crick edge of the ligands and hThyA was compromised, resulting in water exposure. Ligand L2 is particularly advantageous for its highest affinity for MtbThyX and weak affinity for hThyA. The L2:MtbThyX complex is stabilized by a new salt-bridge interaction (COO^- of L2···Arg107 of protein) and a bridging water molecule (between COO^- of L2 and E92 of protein) in the binding pocket. Moreover, our estimated pK_a of +4.5 units of N3 (dUMP) in the MtbThyX catalytic pocket indicated the strong acidic nature of the uracil, corroborating previous experimental and computational claims. These findings provide insights into the protein−ligand binding affinity in atomic detail and a rational approach for inhibitor design against MtbThyX.

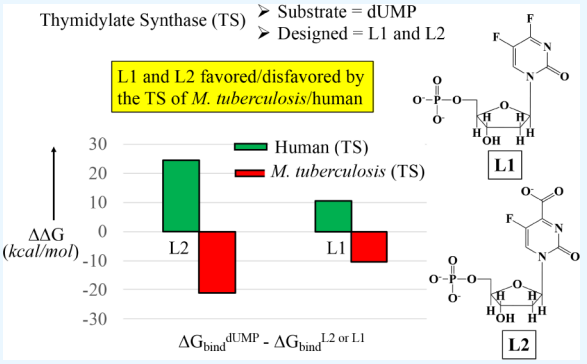

INTRODUCTION

Thymidylate synthase[1,2] is a key enzyme that catalyzes the conversion of deoxyuridine monophosphate (dUMP) to deoxythymidine monophosphate (dTMP) (Figure 1a). As dTMP is a precursor of DNA, inhibition of thymidylate synthase causes "thymine-less" death.[3,4] Thymidylate synthase of *M. tuberculosis* (MtbThyX; homotetrameric protein) is structurally[5−7] and mechanistically[2,8,9] unrelated to its human analogue (hThyA, homodimeric protein) (Figure 1b). Moreover, MtbThyX binds to the deprotonated/enolate form of the substrate (dUMP$^{(d)}$; ionized at N3), contrary to dUMP binding to hThyA.[10−12] Methylenetetrahydrofolate (mTHF) is a cofactor that acts as a methyl group donor to dUMP. MtbThyX requires a flavin adenine dinucleotide (FAD) molecule (sandwiched between dUMP$^{(d)}$ and mTHF) for catalysis, which is not required for hThyA. In the ThyX catalytic pocket, dUMP$^{(d)}$ is stabilized by forming stacking interactions with the flavin group of FAD.[13] Stacking of FdUMP and FAD is evident in the X-ray structure of the MtbThyX complex (Figure 1b). On the other hand, dUMP forms a stacking interaction with methylenetetrahydrofolate (mTHF) in hThyA.[5] In the X-ray structure of the dUMP:-hThyA complex (Figure 1b), antifolate nolatrexed occupied the position of mTHF. Two types of thymidylate synthase

Received: November 19, 2024
Revised: March 3, 2025
Accepted: March 6, 2025
Published: April 4, 2025

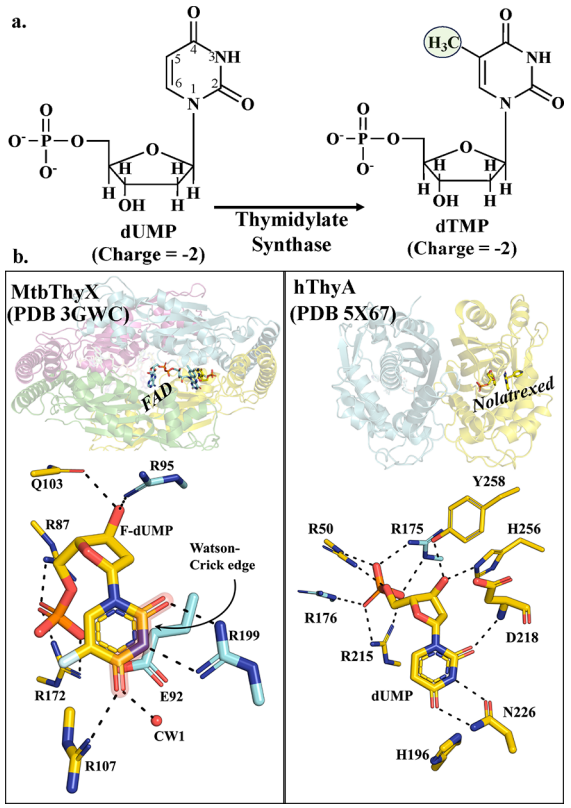

Figure 1. (a) Conversion of dUMP to dTMP is catalyzed by thymidylate synthase. Atom numbers in the uracil ring are explicitly mentioned. (b) Crystal structure of thymidylate synthase from *Mycobacterium tuberculosis*(homotetramer, MtbThyX in complex with FdUMP and FAD) and humans (homodimer, hThyA in complex with dUMP and antifolate nolatrexed). Monomeric units are in cartoon representation and highlighted by different colors. Cofactors FAD/nolatrexed form $\pi-\pi$ stacking interaction with FdUMP/dUMP. Zoomed-in view of the catalytic pocket around FdUMP/dUMP. Key residues (in sticks), network of interaction (shown in black broken lines), and crystal water molecule (CW1 in red sphere), and ligand (F-dUMP, yellow). FAD/nolatrexed is not shown for clarity in the zoomed in view. Watson−Crick edge of FdUMP is highlighted by red surface.

(ThyX, ThyA) are present in *M. tuberculosis*. However, experiments confirmed that pathogenic growth relies only on ThyX.[14,15] Needless to say, ThyX, being essential for pathogenic growth and distantly different from its human analogue, is a well-established pharmacological target. Considerable effort is ongoing to develop substrate- and nonsubstrate-based inhibitors against ThyX.[12,16−20] Fluorine-substituted (FdUMP or fluoro-deoxyuridine monophosphate, Figure 2) is a known substrate-based inhibitor of thymidylate synthase.[21] Anticancer drug 5-fluorouracil (5FU) is converted to FdUMP in the cell but inhibits both ThyX and ThyA.[22,23] Thus, the poor selectivity of FdUMP disqualified its clinical application. On the other hand, naphthoquinones (another class of nonsubstrate-based compounds) displayed selectivity but are limited by cytotoxicity.[24]

Structural,[5,6] biochemical,[10,12] and theoretical studies[11,12] highlighted distinctly different mechanisms of MtbThyX and hThyA activity. The substrate dUMP is stabilized in the catalytic pocket of hThyA, contrary to dUMP$^{(d)}$ in the case of ThyX (Figure 2). Residue E92 is believed to be neutral, and a crystal water molecule (CW1) was shown to be critical for the

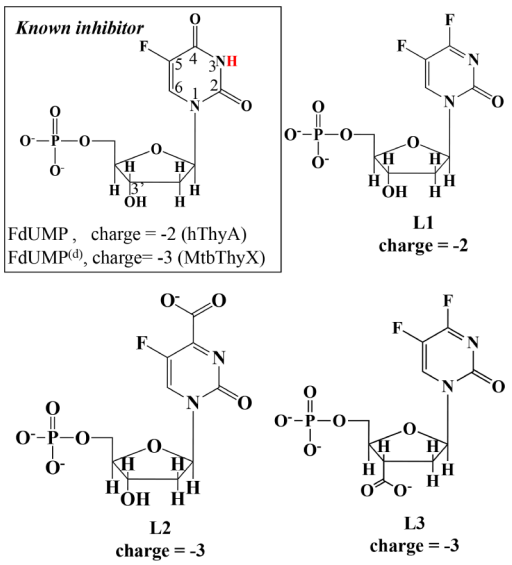

Figure 2. Structure of the known inhibitor FdUMP and its ionized form FdUMP$^{(d)}$. The ionizable proton connected to the N3 atom of FdUMP is highlighted in red. The structure and overall charge of the designed ligands (L1, L2, and L3; does not contain a proton in the N3 atom of the base). Only L2 and L3 contain the carboxylic group.

stability of the MtbThyX: dUMP$^{(d)}$ complex.[6,11,12] The X-ray structures (PDB 5X67 and PDB 3GWC for human and *M. tuberculosis* respectively,[5,6] Figure 1b) are sufficiently good models (resolution ∼2 Å) for computational analysis and uncover the energetics of small molecule binding to the proteins. First, we calculated the pK_a of the N3 atom of dUMP in the MtbThyX binding pocket. The result indicated that the pK_a of N3 of uracil is negative in the MtbThyX binding pocket, attributed to the favorable electrostatic interactions between cationic side chains (Arg199 and Arg107) and the Watson−Crick edge of the uracil ring, corroborating with the previous reports.[10,12] Next, we exploited the difference in the FdUMP (known inhibitor): protein (MtbThyX and hThyA) interaction network and rationalized the design of promising drug-like ligands (Figures 2 and 3) against MtbThyX. The ligand design was guided by comparing experimentally resolved structures, spectroscopic data, biochemical assays, and computational analysis. We report three ligands (L1, L2, and L3) by substituting fluorine and carboxylic groups in FdUMP that do not contain a proton in the Watson−Crick edge of uracil. Alchemical free energy simulations were performed to decipher the energetics of ligand selectivity in MtbThyX and hThyA (Figure 4). L2 was identified as the most promising selective inhibitor scaffold for MtbThyX, and the mode of interactions of L2 in the binding pocket is found to be more or less identical to that in the case of dUMP$^{(d)}$. We showed that besides the known structural differences, the MtbThyX differed distinctly from hThyA in terms of (1) solvent accessibility and (2) the influence of sugar puckering on the substrate/ligand. A relatively dry MtbThyX catalytic pocket stabilized the compact substrate/ligand conformation (boosting C3′-endo), contrary to the relatively wet hThyA that preferred a relatively extended substrate/ligand conformation. The link between energetics (Figure 4) and the atomic interaction network (Figures 5 and 6) provided a deeper understanding of small-molecule selectivity, which may facilitate the rational design of new selective antibiotics against the MtbThyX enzyme.

https://doi.org/10.1021/acsomega.4c10518
ACS Omega 2025, 10, 13966−13976

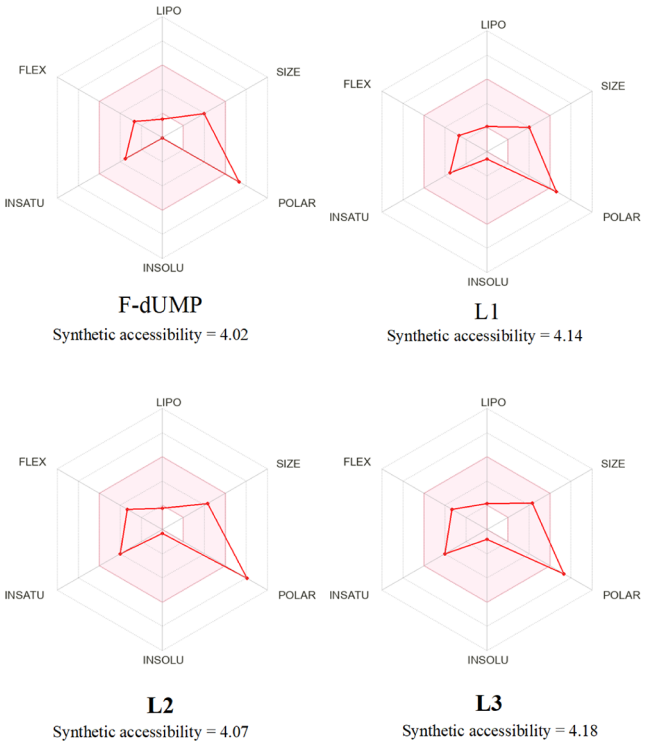

Figure 3. Assessment of drug-likeness. The area shaded in pink represents the optimal range of properties for drug-like molecules (lipophilicity: −0.7 to +5.0, size (molecular weight): 150 to 500 g/mol, polarity (topological polar surface area): 20 to 130 Å^2, solubility: ≤6, saturation (sp^3 carbon): ≥0.25, and flexibility: ≤9 rotatable bonds. All the molecules pass Lipinski's rule of five. The polarity of the ligands is above the desired range. Synthetic accessibility score ranges between 1 (easily synthesizable) and 10 (challenging to synthesize if score >6).

MATERIALS AND METHODS

Molecular Dynamics Setup for Conventional Simulation Study. Structure of thymidylate synthase of human (hThyA in complex with dUMP and nolatrexed, PDB 5X67, resolution of 2.13 Å)[5] and *Mycobacterium tuberculosis*-(MtbThyX; in complex with FdUMP and FAD, PDB 3GWC, resolution of 1.9 Å)[6] was taken from the Protein Data Bank. The protein was kept at the center, and an equilibrated cubic water box was overlaid so that the minimum distance of the protein to the box edges was 1.2 nm. The water molecules that overlapped with the protein were removed. The water molecules (267 and 422 for hThyA and MtbThyX, respectively) resolved in the crystal structures were considered in our MD model. Our model for MD simulations included the full protein (dimeric and tetrameric hThyA and MtbThyX, respectively) in a box of water (Tables S1 and S2). Counterions (Na^+) were added to ensure charge neutrality of our simulation box. To ensure convergence, we considered various models (Tables S1 and S2) by varying the box size (solvation), protonation state of titratable residues, monovalent salt concentration (NaCl = 0 or 150 mM), etc. Periodic boundary conditions were employed during MD simulations. The particle mesh Ewald[25] method was used to calculate the long-range electrostatic interactions with a short-range cutoff of 1.2 nm. The van der Waals interactions were truncated at a cutoff distance of 1.2 nm. The system was energy minimized (step size ∼0.01 nm, steps ∼50000) by employing the steepest descent algorithm. The energy-minimized simulation box was subjected to a two-phase equilibration (first phase: 500 ps in NVT ensemble; second phase: next 10 ns in NPT ensemble). After equilibration, the simulation was extended for production dynamics in the NPT ensemble for a minimum of 100 to a maximum of 400 ns. The production dynamics were used for data collection. The temperature and pressure of the system were maintained at 310 K and 1 bar, respectively. The temperature was controlled by using velocity rescaling[26] for the nonhydrogen atoms, with a coupling coefficient of 0.1 ps; pressure was controlled by a Parrinello−Rahman barostat[27,28] with a time constant of 5 ps. Hydrogen atoms connected to heavy atoms were restrained using the LINCS algorithm,[29] and a 2 fs time step was used for MD. The CHARMM36m force field[30,31] was used to model the biomolecular interactions.

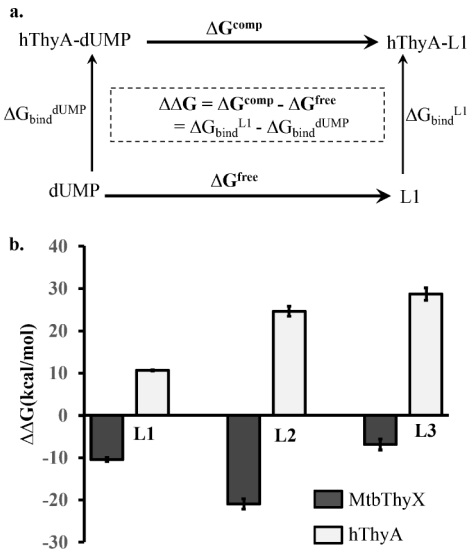

Figure 4. (a) Thermodynamic cycle for estimating the difference in binding affinity of dUMP and L1 to the catalytic pocket of hThyA. The vertical arms correspond to the ligand binding to hThyA. The free energy along the horizontal arms was calculated that corresponds to the alchemical transformation of dUMP to L1 in complex with hThyA (upper arm) and free (lower arm) in water. The binding affinity difference ($\Delta\Delta G$) is calculated as $\Delta\Delta G = \Delta G^{comp} - \Delta G^{free} = \Delta G^{L1}_{bind} - \Delta G^{dUMP}_{bind}$. (b) The difference in binding free energy ($\Delta\Delta G$) in the MtbThyX (dark gray bar) and hThyA (light gray bar) is plotted for all the ligands relative to dUMP. Error in s.e.m.

The same force field was used in our previous work,[11] and the calculated $\Delta\Delta G$ (FdUMP versus dUMP in hThyA/MtbThyX) was shown to be in excellent agreement with experimental results, thus justifying the reliability of the adopted force field. The CHARMM-modified TIP3P model[32] was used to describe the water molecules. CGenFF[33] was used to model the deprotonated substrate and the designed ligands. Designed ligands are either replaced in place of dUMP/FdUMP (in X-ray structures of hThyA/MtbThyX) or alchemically generated in the catalytic pocket during the course of the simulation. The same MD protocol was employed to study the dynamics of the free substrate/ligand in a water box. GROMACS software[34] was used to run simulations. CGenFF[33] was utilized to define the ligands and to generate input files for GROMACS.[34] Hybrid structure and topology files were created using the pmx command-line interface.

https://doi.org/10.1021/acsomega.4c10518
ACS Omega 2025, 10, 13966−13976

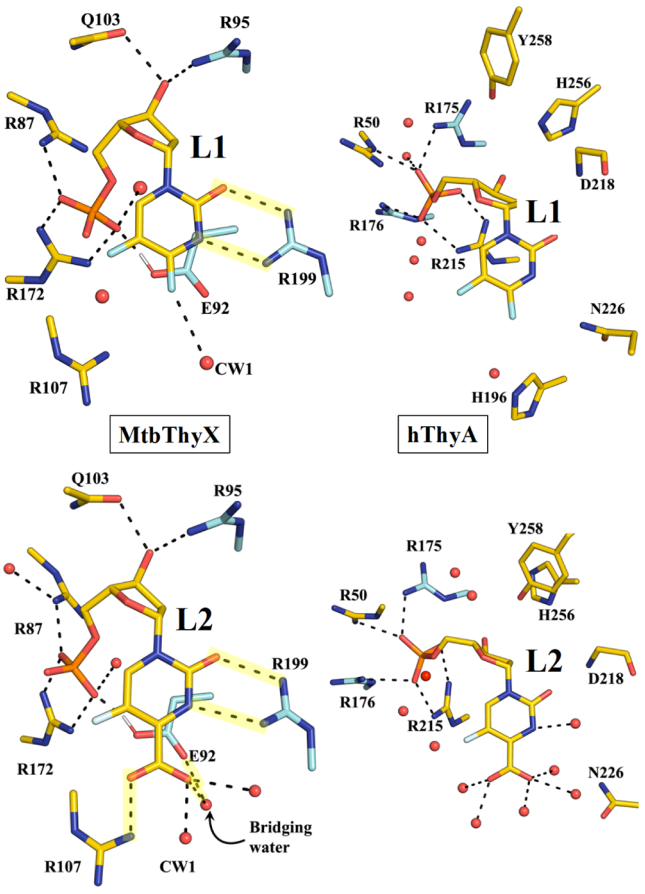

Figure 5. Zoomed-in view of the ligand binding pocket of MtbThyX (left) and hThyA (right). The ligands L1 and L2 are explicitly mentioned. Key residues are depicted as sticks, while the black broken line indicates the interaction network. Key distances are highlighted in yellow, and water molecules are represented by red spheres.

Protonation State of Key Residues in MtbThyX Model. Protonation states of the titratable amino acid side chains (Glu, Asp, His, Lys, Arg) were assigned by combining various methods, including visual inspection of the local environment in the X-ray structures, pK_a calculations, and previous studies.[10,12] PROPKA[35,36] predicted the pK_a value of +10.2 for the E92 side chain of MtbThyX. Thus, we considered neutral E92 in the MtbThyX complex, which is consistent with the short distance of 2.6 Å between the E92 side chain and the phosphate of 5F-dUMP observed in the X-ray structure,[6] NMR experiments,[10] and computational analysis.[11,12] The side chain pK_a = 4.3 (at neutral pH = 7.0) of the free glutamic acid in water is lower than the pK_a = 7.2 of the phosphate of UMP.[37] The situation changes significantly in the complex because: (1) the phosphate group of F-dUMP interacts with the side chains of two arginine residues (R87, R172), forming salt bridges that stabilize the deprotonated form of the phosphate. This interaction lowers the pK_a of the phosphate moiety. (2) The proximity of approximately 2.6 Å between the phosphate group of F-dUMP and the side chain of E92 increases the pK_a of E92. In a previous study,[11] we conducted simulations using two models: model 1 (which features a neutral Glu92 and a charged phosphate) and model 2 (which includes a neutral phosphate and a charged Glu92). Our findings indicated that model 1 more accurately reproduced the X-ray structure. In contrast, simulations using model 2 changed the orientation of the phosphate group and disrupted key salt bridge interactions with R172. Thus, we concluded that the neutral form of E92 is the most suitable representation in the MtbThyX pocket as it maintains the integrity of the ligand binding pocket observed in the experimentally resolved structure during the molecular dynamics (MD) simulations. In the case of L3 in MtbThyX, two protonation states of E92 were modeled (protonated: GLH and deprotonated: GLU) for simulations, and the individual ΔG^{comp} values are reported in Supporting Information (Table S2). Direct salt-bridge interactions between the phosphate of FdUMP and two arginine residues (R87 and R172) in the MtbThyX significantly lower the pK_a, which could be attributed to the preferential ionization of phosphate. Simulations with different protonation states of the histidine (charged or neutral), i.e., His261 of hThyA (PROPKA: pK_a = +7.6) and His194 of MtbThyX (PROPKA: pK_a = 7.49) confirmed that the results are independent of the histidine protonation state (Table S2).

Alchemical Simulations for Relative Binding Free Energy Estimation. Binding free energy differences ($\Delta\Delta G$) of the substrate and ligand binding to the thymidylate synthase were estimated from alchemical simulations by employing an appropriate thermodynamic cycle (Figures 4a and S1). Final structures of the complex (viz., dUMP:hThyA, dUMP$^{(d)}$:MtbThyX) from the standard MD production run were subjected to alchemical simulations. In the alchemical simulation (horizontal arm of Figure 4a), the substrate (dUMP) was slowly transformed to L1 by altering the force

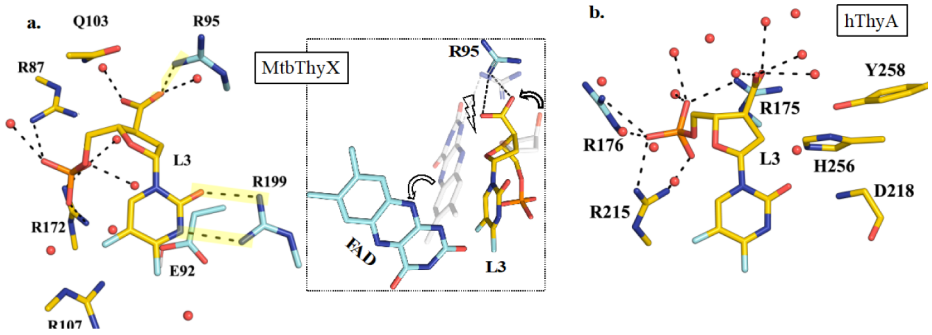

Figure 6. Zoomed-in view. (a) L3 in the MtbThyX binding pocket. Disruption of FAD:L3 stacking interaction is highlighted in the broken box. Transparent gray sticks (X-ray structure, part of FdUMP, FAD, and R95 side chain is shown for clarity). (b) L3 in hThyA binding pocket. Key residues are represented as sticks, and the black broken lines indicate the key interaction network, which is also highlighted in yellow. Water molecules are depicted as red spheres.

https://doi.org/10.1021/acsomega.4c10518
ACS Omega 2025, 10, 13966−13976

field parameters (alchemical transformation). The alchemical free energy change (ΔG^{comp} and ΔG^{free}) was estimated by the Bennett acceptance ratio (BAR) method.[38] The difference between ΔG^{comp} and ΔG^{free} estimated the binding free energy difference ($\Delta\Delta G$). A hybrid structure of substrate/ligand and the topology file was generated using the PMX package.[34] A coupling coordinate "λ" gradually modifies the force field parameters of the hybrid substrate/ligand (simultaneously alters the electrostatic, van der Waals, and bonded terms). Thus, a slow variation of λ from 0 to 1 can transform the dUMP to L1. Note a value of λ other than 0 or 1 represents an unphysical state (mixture of dUMP and L1) and accounts for the term alchemical transformation. λ alters the energy function (E) and modifies the Hamiltonian ($E = \lambda E(\mathrm{L1}) + (1-\lambda)\, E(\mathrm{dUMP})$) and connects the two physically realizable end states as λ varies from 0 → 1. Fifty-one equally spaced λ values and a soft-core potential were used for smooth alchemical transformation (λ: 0 → 1). The free energy difference (ΔG_{ij}) between two neighboring λ windows (say, λ = "i" and "j") was estimated by the BAR method.[38] The total alchemical free energy difference (ΔG^{comp}) between the end states ($\lambda = 0$ and $\lambda = 1$) is simply the sum of ΔG_{ij}'s. The same methodology was adopted to calculate the alchemical transformation in the absence of protein (ΔG^{free}). The statistical error associated with ΔG^{comp} or ΔG^{free} was computed by the BAR estimator implemented in GROMACS.[34] The relative free energy ($\Delta\Delta G$) is calculated as $\Delta\Delta G = \Delta G^{comp} - \Delta G^{free}$. The above methodology and use of an appropriate thermodynamic cycle estimated the binding free energy difference between any two ligands and the protein of interest.

dUMP versus dUMP$^{(d)}$ Preference in the MtbThyX and pK_a Estimation. The deprotonated substrate, i.e., dUMP$^{(d)}$ is believed to be stabilized in the MtbThyX catalytic pocket, which is supported by (1) the short distance of 2.8 Å between N3 of dUMP and Arg199 observed in the X-ray structure,[6] (2) NMR experiments,[12] and (3) simulations.[12] Experimentally determined pK_a of the N3 atom of dUMP (free in water) has been reported to be +9.3 units.[39]

Thus, at neutral pH, the dUMP is relatively more stable (by ∼+13 kcal/mol) than its N3-deprotonated form dUMP$^{(d)}$ in aqueous solution. Needless to say, the dUMP/dUMP$^{(d)}$ equilibrium in aqueous solution will strongly favor the dUMP population. The effect of the MtbThyX on the dUMP/dUMP$^{(d)}$ equilibrium was examined by alchemical free energy calculations, in which the dUMP$^{(d)}$ was alchemically transformed into the dUMP. These calculations were repeated in the presence and absence of MtbThyX, which allows the relative binding free energies of dUMP and dUMP$^{(d)}$ to be evaluated from a standard thermodynamic cycle. The free energy change for dUMP$^{(d)}$ → dUMP transformation in the presence (ΔG_1^{comp}) and absence (ΔG_1^{free}) of MtbThyX is reported in Table 1. A harmonically restrained Na^+ counterion (force constant = 2 kcal mol^{-1} Å^{-2}) was also transformed into a dummy atom to maintain the charge neutrality of the simulation box. Calculations were repeated by varying the spring constant and location of the counterion (15 or 25 Å away from the N3 atom of the mutating ligand). Estimated $\Delta\Delta G_1 \sim +25$ kcal/mol indicated that MtbThyX strongly prefers dUMP$^{(d)}$ relative to dUMP (Table 1). As anticipated, the deprotonated uracil dUMP$^{(d)}$ is strongly favored in MtbThyX. It is worth mentioning that the calculated strong preference of +25 kcal/mol by MtbThyX in favor of dUMP$^{(d)}$ relative to dUMP could significantly shift the overall equilibrium in favor of the dUMP$^{(d)}$.

Table 1. Alchemical Free Energy Change (kcal/mol) in the MtbThyX Binding Pocket (ΔG_1^{comp}) and Free in Water (ΔG_1^{free}), Errors are s.e.m[a]

	Alchemical transformation: dUMP$^{(d)}$ (N3$^-$) → dUMP (N3−H)		
	MtbThyX (ΔG_1^{comp})	Water (ΔG_1^{free})	$\Delta\Delta G_1 = \Delta G_1^{comp} - \Delta G_1^{free}$
Trial 1	214.7 ± 0.13	188.7 ± 0.05	26.0 ± 0.14
Trial 2	215.4 ± 0.36	188.5 ± 0.04	26.9 ± 0.36
Trial 3	213.5 ± 0.37	188.7 ± 0.09	24.7 ± 0.38
Trial 4	210.7 ± 0.25	188.7 ± 0.03	22.0 ± 0.2
$\Delta\Delta G_1$ (Average)			24.9 ± 1.03

[a]The uncertainty in $\Delta\Delta G_1$ is estimated by propagation of individual uncertainties of ΔG_1^{comp} and ΔG_1^{free}. Trials 1−4 indicated independent simulations differing in starting velocity and solvation.

The relative binding free energy in the vacuum was estimated by performing MM/PBSA calculations on the end-point trajectories of the protein: ligand complexes (embedded in a dielectric = 1). The difference in the calculated binding affinities estimated the relative binding free energy in a vacuum; $\Delta\Delta G_1^{Vac} = \Delta G_{bind}^{Vac,dUMP} - \Delta G_{bind}^{Vac,dUMP(d)}$. The estimated $\Delta\Delta G_1^{Vac} = 18.5 \pm 2.0$ kcal/mol (estimated from eight end-point trajectories of four independent trials) was subtracted from the average $\Delta\Delta G_1$ value (Table 1) to remove force field uncertainties. A similar approach of subtracting the vacuum-free energy difference has been shown to improve the relative binding free energy estimate.[12] The shift of the pK_a of dUMP in response to the change in the local environment (from the solvent to the binding pocket of MtbThyX) obeys the following equation:

$$pK_a^{Prot} - pK_a^{Sol} = -\Delta\Delta G/2.303RT$$

where $\Delta\Delta G = \Delta\Delta G_1 - \Delta\Delta G_1^{Vac}$, R, and T are free energy difference (+6.4 kcal/mol), gas constant (1.987 cal mol^{-1} K^{-1}), and temperature (310 K), respectively. Using the experimental $pK_a^{Sol} \sim +9.3$ of N3 of dUMP in water,[39] the pK_a of dUMP in MtbThyX is estimated to be 4.5 units, indicating the strong acidic nature of uracil in the MtbThyX pocket, in agreement with previous NMR experiments,[10] X-ray structure,[6] and computational analysis.[11,12]

Thus, the severe shift of N3 pK_a is attributed to the proximity of R199 and dUMP$^{(d)}$ (as observed in the FdUMP-bound X-ray structure, depicted in Figure 1b).

Thermodynamic Cycles for Free Energy Calculations. We have considered a total of five ligands shown in Figure 2 (substrate in two different forms: dUMP and dUMP$^{(d)}$ and three designed ligands: L1, L2, and L3). Out of these ligands, dUMP and L1 have an overall charge of −2, whereas dUMP$^{(d)}$, L2, and L3 have an overall charge of −3. For hThyA, we calculated the alchemical free energy change for dUMP → L1 or L2 or L3 transformation in the presence (ΔG^{comp}) or absence of the protein (ΔG^{free}) and reported the binding free energy difference ($\Delta\Delta G$) (Figure 4a). Note, dUMP (charge −2) → L2 or L3 (charge −3) transformation in hThyA also includes a transformation of a chloride ion into a dummy to ensure charge neutrality throughout the alchemical simulations. In the case of MtbThyX, we adopted two different approaches for $\Delta\Delta G$ calculation. In approach 1, we performed

https://doi.org/10.1021/acsomega.4c10518
ACS Omega 2025, 10, 13966−13976

dUMP$^{(d)}$ → L2 or L3 transformation and added the averaged alchemical free energy change for dUMP$^{(d)}$ → dUMP (Table 1) for comparing the substrate (dUMP) versus L2/L3 binding to MtbThyX (Figure S1). In approach 2, we started with the MtbThyX:L1 complex and calculated the alchemical free energy associated with the transformation of L1 → dUMP (Figure S1).

Sampling and Convergence of Free Energies. Standard molecular dynamics simulations for every system were repeated a minimum of three times and a maximum of six times by varying the initial velocities, solvation size, and salt concentrations (in the presence of 150 mM or the absence of NaCl). Sampling of a minimum of 100 ns to a maximum of 400 ns production dynamics was considered for structural analysis (MtbThyX:dUMP$^{(d)}$ = 400 ns, MtbThyX:L1= 200 ns, MtbThyX:L2 = 190 ns, MtbThyX:L3= 140 ns, hThyA:dUMP = 270 ns, hThyA:L1 = 300 ns, hThyA:L2 = 400 ns, and hThyA:L3= 150 ns). After standard production dynamics was established, alchemical simulations were performed. The alchemical transformation includes additional simulations of 51 equally spaced λ windows. For alchemical simulations, we adopted two different sampling strategies (3 or 10 ns per λ window). Thus, a single alchemical calculation includes a total of either 153 or 510 ns of MD. A total of ∼3.25 μs of conventional MD simulation followed by ∼17 μs of alchemical simulations (total ∼20.25 μs sampling) ensured good convergence and reasonable statistical error (less than 1.5 kcal/mol; Tables S1 and S2). Data from various independent trajectories (ΔG_1^{comp}, ΔG_1^{free}) are averaged and reported as $\Delta\Delta G$ (Table S3). The standard error of the mean (sem) was reported as an error associated with alchemical free energies (ΔG^{comp} and ΔG^{free}). The individual errors were propagated and assigned as error for $\Delta\Delta G$. The positive/negative sign of $\Delta\Delta G = \Delta G_1^{comp} - \Delta G_1^{free}$ indicates the preference, whereas the magnitude indicates the strength of preference. For example, for A → B alchemical transformation, a positive/negative value of $\Delta\Delta G$ indicates that "A" binding to the protein is favored/disfavored relative to "B", while the magnitude of $\Delta\Delta G$ indicates the strength of the preference. Good overlap of the probability distribution function between two neighboring λ-windows ensured reversibility and efficiency of the calculated free energies (Figures S2−S4).

RESULTS

Structural and Mechanistic View of the Catalytic Pocket of the Enzyme. The objective of this work is to design promising selective inhibitor(s) against thymidylate synthase of *Mycobacterium tuberculosis*(MtbThyX) using a known nonselective inhibitor FdUMP (Figure 2) as a template. The knowledge of the catalytic pocket and the mechanism is relevant for the rational design of promising inhibitors. X-ray structures[5,6] suggested two distinct structural features of the substrate binding pocket (hThyA and MtbThyX) to be particularly relevant for designing selective inhibitors in the thymidylate synthase (Figure 1b). First, the interaction network between the Watson−Crick edge of the pyrimidine base and the protein is distinctly different in the host (hThyA) and pathogenic (MtbThyX) enzyme. MtbThyX involves cationic side chains (R199, R107) contrary to the polar residues (side chain and main chain of N226 and D218, respectively) in hThyA for interacting with the uracil base of the substrate (Figure 1b). The proximity of R199 and pyridine base in the X-ray structure[12] and our pK_a calculations (see Materials and Methods) showed that the pyridine base is deprotonated (dUMP$^{(d)}$; deprotonation at N3) in MtbThyX contrary to its keto form (dUMP) in hThyA, corroborating previous experimental[10] and theoretical studies.[11,12] Second, the ribose −OH of the nucleotide is placed in a positively charged pocket in MtbThyX (involving R95 and Q103 side chains), contrary to a polar pocket in hThyA (involving H256 and Y258). We have noticed that the model of neutral histidine (H256: proton either in epsilon or delta position) strongly affects the stability of OH(Y258)···O3′(dUMP) hydrogen bond. The OH(Y258)···O3′(dUMP) hydrogen bond is preserved for the system containing H256-δ (proton at delta position). We have estimated the free energies for both models and found that the relative binding affinity ($\Delta\Delta G$, dUMP vs L1) was almost identical ($\Delta\Delta G^{His\text{-}\epsilon}$ = 9.23 ± 0.14, $\Delta\Delta G^{His\text{-}\delta}$ = 8.92 ± 0.8 kcal/mol). In summary, the dUMP$^{(d)}$ is the substrate for MtbThyX, where the nucleoside forms direct interaction primarily with the cationic side chains (R107, R199, and R95; Figure 1b). On the other hand, hThyA binds to dUMP, where the nucleoside establishes interaction only with the polar functional groups (Figure 1b), which demands the presence of −NH in the uracil for the stability of the hThyA:dUMP complex. Thus, it can be argued that the known inhibitor (FdUMP) can bind to both MtbThyX and hThyA in its deprotonated FdUMP$^{(d)}$ (enolate, deprotonated form at N3) and FdUMP (keto) forms, respectively, thus nonselective in nature. Previously, we showed that both hThyA and MtbThyX favor inhibitor (FdUMP) binding relative to the substrate (dUMP) primarily due to the favorable electrostatic interactions.[11] Interestingly, FdUMP was found to be a more potent inhibitor of hThyA (K_i, 2 nM) relative to MtbThyX (K_i, 100 nM),[23] thus disqualified for clinical application against *M. tuberculosis*. FdUMP can covalently bind to human thymidylate synthase and its cofactor,[40,41] which may also contribute to the higher affinity for hThyA. A conserved water molecule (CW1 of Figure 1b) was reported in the X-ray structure of MtbThyX, which has been shown to be stable in the MD trajectories and key for the binding pocket integrity.[11] Moreover, simulations suggested that CW1 can bridge between the inhibitor (O4 of FdUMP) and the neutral E92 residue of MtbThyX.

Rationale of Inhibitor Design, Drug-Likeliness, and Structural Stability. We redesigned the nonselective FdUMP inhibitor (Figure 2) to achieve selectivity. The new ligands are supposed to (1) be favored and disfavored by MtbThyX and hThyA, respectively and (2) display strong affinity to the target MtbThyX. Our strategy includes two primary modifications in the FdUMP$^{(d)}$: (1) removal of the proton from the Watson−Crick edge of the pyrimidine and (2) incorporation of negative charge on the nucleoside. The absence of a proton in the pyrimidine −N3 is advantageous for binding to MtbThyX (bypassing the deprotonation requirement of the pyrimidine ring) but disfavored binding to hThyA (disrupt N3−H: protein interaction). Thus, the same modification is likely to ensure selectivity. Moreover, the incorporation of negative charge in the nucleoside is likely to improve the strength of binding by forming new salt-bridge interactions with the arginine side chains (R107 or R95) of MtbThyX. Removal of hydrogen from N3 was compensated by a double bond (N3═C4) and substitution of ketone oxygen (C4═O4) with fluorine (L1 and L3 of Figure 2) or a carboxylic group (L2 of Figure 2). As expected, the empirical pK_a predictor MolGpKa[42] confirmed that the carboxylic group of the ligands

https://doi.org/10.1021/acsomega.4c10518
ACS Omega 2025, 10, 13966−13976

(L2 and L3) is likely to be deprotonated ($-COO^-$) in an aqueous medium (pK_a < 3, Figure S5) at pH 7. Thus, it can be argued that the negatively charged COO^- will be stabilized further in the cationic binding pocket of the protein, particularly in MtbThyX. The carboxylic group in C4 (as in L2) or in the ribose sugar (as in L3) has been anticipated to introduce new salt-bridge interactions with R107 or R95 in the MtbThyX catalytic pocket (Figure 1b).

The drug-likeness properties of the designed ligands (L1, L2, and L3) were determined (Figure 3, and Table S4) using the SwissADME tool.[43] All the ligands (L1, L2, L3, and FdUMP) met the drug-likeness criteria imposed by Lipinski's rule[44] of five. However, only L1 and L3 could qualify for the Ghose filter.[45] The low synthetic accessibility score (i.e., less than 6)[46] of all the ligands indicated that the molecules are easy to synthesize. L1 has been predicted to be advantageous due to lower molecular weight (<350 g/mol) and polarity (charge = −2) relative to L2 and L3 (MolWt > 350 g/mol, charge = −3).

MD simulations showed that the ligands in the free state or in the hThyA pocket are more extended relative to the MtbThyX-bound complex (Table 2). In the extended conformation (free or hThyA complex), the phosphate moiety of the ligand bent away from the base, whereas the same bent back toward the base in the compact conformation (in the MtbThyX complex). MtbThyX-induced ligand compactness is noticeable, supported by the smaller "P...C4" distance (Table 2). In L3, the carboxylic group is present in the ribose sugar. Thus, the compaction of L3 increased the "P···COO" distance in the L3:MtbThyX complex (Table 2). The ribose sugar in RNA is known to pucker predominantly in the C3′-endo conformation, contrary to primarily the C2′-endo conformation in DNA (Figure S6). The difference in the sugar puckering distinctly alters the P···O3′ distance, which is smaller for RNA relative to its DNA analogue (Figure S6). We showed that the P···O3′ distance in the ligands is larger in MtbThyX relative to hThyA (Table 2). Interestingly, after revisiting the X-ray structures, we found that the same is true for FdUMP in the MtbThyX (PDB 3GWC, P···O3′ = 5.9 Å) and dUMP in hThyA (PDB 5X67, P···O3′ = 5.0 Å), corroborating our claim. Thus, it can be argued that the sugar puckering is strongly influenced by the nature of the protein (MtbThyX favors C2′-endo and hThyA favors C3′-endo conformation). Furthermore, an inverse correlation between the sugar puckering (indicated by the P...O3′ distance) and the P···C4 distance is evident (Table 2). As expected, the degree of solvation for the free ligands is much higher (>30 water molecules) than in the protein-binding pocket (hThyA: 6−14 and MtbThyX: 3−8 water molecules). Note that the catalytic pocket in MtbThyX is relatively dry compared to hThyA.

Table 2. Trajectory Averaged Key Interatomic Distances (in Å) and the Total Number of Water Molecules around 3.4 Å of the Ligand Are Given[a]

	Ligand	Water	MtbThyX	hThyA
P···C4 Distance (Å)	dUMP	7.81 ± 0.10	5.85 ± 0.70	8.26 ± 0.05
	dUMP$^{(d)}$	7.69 ± 0.04	5.13 ± 0.10	ND
	L1	7.57 ± 0.32	4.89 ± 0.32	7.94 ± 0.21
	L2	7.86 ± 0.04	5.33 ± 0.15	8.17 ± 0.11
	L3	7.19 ± 0.15	5.28 ± 0.60	8.03 ± 0.18
P···COO Distance (Å)	L2	9.03 ± 0.05	6.59 ± 0.37	8.89 ± 0.17
	L3	5.26 ± 0.05	5.73 ± 0.37	5.25 ± 0.12
P···O3′ Distance (Å)	dUMP	5.13 ± 0.13	5.61 ± 0.29	4.45 ± 0.67
	dUMP$^{(d)}$	5.17 ± 0.09	5.71 ± 0.16	ND
	L1	5.21 ± 0.10	5.72 ± 0.11	4.68 ± 0.52
	L2	5.06 ± 0.05	5.64 ± 0.28	4.89 ± 0.52
Solvation (H_2O around 3.4 Å of the ligand)	dUMP	32.08 ± 2.54	5.76 ± 0.98	6.40±2.14
	dUMP$^{(d)}$	33.60 ± 2.53	3.37 ± 0.95	ND
	L1	31.88 ± 2.65	2.65 ± 0.87	7.37 ± 1.56
	L2	34.34 ± 2.42	4.82 ± 1.06	10.45 ± 2.96
	L3	33.02 ± 2.57	8.36 ± 1.5	13.68 ± 3.92

[a]Error is the standard deviation. "ND" stands for not performed.

The similarity between MD and the template X-ray structure was assessed by plotting the root-mean-square deviation (rmsd) of protein-heavy atoms relative to the X-ray structure (Figures S7 and S8). The plateau in the RMSD versus time plot (after 40 ns) indicated structural convergence. Trajectory-averaged small RMSD (∼2 Å) for different models indicated that protein structures in the MD are more or less reproducing the template X-ray structures. As expected, the simulation of dUMP$^{(d)}$:MtbThyX and dUMP:hThyA complexes reproduced the interaction network observed in the X-ray structure (Tables S5 and S6 and Figure 1b).

Thermodynamics of Substrate versus Inhibitor Selectivity. To calculate the binding free energy difference ($\Delta\Delta G$) of the ligand (L1 or L2 or L3) and the substrate (dUMP) to the thymidylate synthase (MtbThyX and hThyA), we performed alchemical molecular dynamics simulations of substrate and ligand-bound complexes using the X-ray structures (PDB 3GWC, PDB 5X67)[5,6] as starting structures. These calculations computed the change in binding affinity upon dUMP → Ligand (L1 or L2 or L3) transformation in the catalytic pocket of thymidylate synthase (MtbThyX and hThyA). Employing an appropriate thermodynamic cycle (Figures 4a and S1), the relative binding affinities ($\Delta\Delta G$) were calculated (Figure 4b). The relative binding free energies in a vacuum were subtracted to remove the force field bias. The positive/negative $\Delta\Delta G$ indicates that the protein favors/disfavors the substrate relative to the ligand(s), and the magnitude indicates the strength of preference. The results unveil some remarkable features (Figure 4b). First, the designed ligands are preferred over the substrate (dUMP) for binding to MtbThyX. However, the strength of preference follows the order L2 > L1 > L3, suggesting that L2 is the strongest binder for MtbThyX. Second, the ligands are found to be strongly disfavored for binding to the hThyA catalytic pocket relative to dUMP. L1 is disfavored by ∼9 kcal/mol, which rises to more than 20 kcal/mol for L2 and L3 in the hThyA. Third, L2 is particularly interesting, as it is strongly disfavored and favored by hThyA and MtbThyX, respectively.

Structural Basis of Selectivity. MtbThyX offers a relatively dry pocket compared to that of hThyA for ligand binding (Table 2). Thus, the favorable protein:ligand electrostatic interactions were amplified by the lower dielectric environment, thereby boosting the strength of binding in MtbThyX. On the other hand, major distortion of the catalytic pocket architecture was observed in the hThyA:ligand complexes. The strength of discrimination disfavoring ligands ($\Delta\Delta G$ = +ve) is attributed to the lack of hThyA:ligand hydrogen bonding (as anticipated) that causes water exposure of the catalytic pocket.

The local interaction network of the designed ligands, particularly "L2" in the MtbThyX binding pocket (Figure 5), is more or less identical to that of the X-ray structure (PDB

https://doi.org/10.1021/acsomega.4c10518
ACS Omega 2025, 10, 13966−13976

3GWC, Figure 1). As anticipated, L2 forms very stable electrostatic interactions with R199 and R107 of MtbThyX (Figure 5, Table S5). The permanent charge on the COO^- of L2 resulted in a new salt-bridge interaction with R107 in MtbThyX. MD trajectories identified a new water molecule that bridged between neutral E92 of the protein and the COO^- of L2, thus acting as a structural water and never being exchanged with the bulk water throughout the trajectory. On the contrary, L2 in the hThyA forms a relatively weaker interaction, involving only the side chain of D218 and fulfilling the hydrogen bonding requirements by interacting with water molecules (Figure 5, Table S6). Favorable binding of L1 to MtbThyX relative to hThyA is attributed to the favorable electrostatic contact between L1 and R199 in the former (Figure 5, Table S5). However, the anticipated fluorine···R107 interaction was not found in the L1:MtbThyX complex. The fluorine of L1 was found to interact with a water molecule. Water-mediated interaction between R107 and L1 was occasionally observed in the trajectory.

The substitution of ribose −OH by a bulky $-COO^-$ group in L3 formed the anticipated COO^-(L3)···R95 salt-bridge interaction (Table S5) but severely compromised the L3:FAD stacking interaction (due to steric reasons) in MtbThyX (Figures 6 and S9). Disruption of the binding pocket integrity is evidenced by the entry of water molecules in the L3:MtbThyX binding pocket (Table 2). Note, the ribose −OH of $dUMP^{(d)}$ or L1 or L2 was placed in a dry pocket (no water molecule within 3.4 Å) of MtbThyX. Thus, substitution of polar −OH by bulky negatively charged $-COO^-$ in the low dielectric environment disrupts the electrostatics, causing severe distortion of the MtbThyX binding pocket. Two water molecules were found to solvate the COO^-(L3) group in MtbThyX (Figure 6). The importance of R95 in stabilizing the integrity of the MtbThyX binding pocket is evident, and its energetics will be reported elsewhere. The L3:MtbThyX complex highlighted that the favorable R95···COO^- interaction is offset by severe disruption of the catalytic pocket architecture (losing L3:FAD stacking, solvent exposure). L3 binding to hThyA is strongly penalized primarily due to the loss of R50···phosphate salt-bridge interaction along with the disruption of expected uracil:protein interactions (Table S6).

The compromise of interaction between the Watson−Crick edge of ligands and hThyA was evident and attributed to the estimated discrimination strength. On the other hand, favorable electrostatic interaction between the negatively charged ligand and the cationic binding pocket of MtbThyX is attributed to the preferable binding, which is noticeable for L2. L3 in the catalytic pocket of both MtbThyX and hThyA strongly disrupted the local interaction network, primarily due to the steric effect of bulky COO^- in the ribose sugar. The results encourage the synthesis of L2 and L1 and experimentally verify the predictions as selective inhibitors against MtbThyX.

DISCUSSION

Our study indicated that the binding pocket of MtbThyX stabilizes the deprotonated $dUMP^{(d)}$ (Table 1), whereas the neutral dUMP is the preferred substrate of hThyA, which is in agreement with the previous experimental and simulation studies.[10−12] The ionized form of $dUMP^{(d)}$ in MtbThyX was supported by the negative value of pK_a of the N3 atom (dUMP) obtained from our calculated relative binding affinity. Next, we designed three inhibitors (L1, L2, and L3, Figure 2) against MtbThyX by mimicking the deprotonated substrate $dUMP^{(d)}$. The calculations showed that MtbThyX favored ligand binding relative to neutral substrate dUMP in the order L2 > L3 > L1 (Figure 4). The ligands are found to be disfavored by hThyA relative to its substrate dUMP in the order L2 > L1 > L3 (Figure 4). Thus, L2 (charge = −3) is predicted to be the most promising selective inhibitor (most favored and strongly disfavored by MtbThyX and hThyA, respectively) among the designed ligands. L2 preserved the same interaction mode (as in the case of $dUMP^{(d)}$) with R107 and R199 in the MtbThyX binding pocket (Figure 5). L1 (charge = −2) is also selective and advantageous due to its smaller overall charge. On the other hand, L3 is limited by poor affinity to MtbThyX as the bulky $-COO^-$ in the ribose sugar disrupts the integrity of the binding pocket (Figure 6). The catalytic pocket of MtbThyX is relatively desolvated (dry) compared to that in hThyA (wet) (Table 2). Furthermore, the nature of the catalytic pocket (hThyA or MtbThyX) modulates the compactness of the ligands by fine-tuning the sugar puckering. The ligands are more compact (short phosphate··· C4 distance) in MtbThyX relative to hThyA (Table 2).

In summary, we propose two competitive inhibitors (L1 and L2, which do not require deprotonation) to dUMP against MtbThyX. A simple substitution of fluorine (L1) or a carboxylic group (L2) in the place of C4═O in the template FdUMP, in principle, can satisfy the bonding and stacking requirements in MtbThyX. Simulations indeed showed that the key interactions and the stacking with the flavin ring were stable throughout the MD trajectories. These results encouraged the synthesis and experimental verification of L1 and L2 as selective inhibitors of MtbThyX. We believe that L1 and L2 can be used as templates for the development of new ThyX inhibitors. The calculated physicochemical properties suggest that the designed ligands have drug-like characteristics. Additionally, the calculated relative binding affinities ($\Delta\Delta G$) indicate that these ligands preferentially bind to MtbThyX compared to the substrate dUMP. However, it is important to note that this study does not establish a direct relationship between the physicochemical properties and the binding affinities. Although the adopted alchemical binding free energy calculations are one of the most popular and accurate methods for calculating relative ligand-binding affinities,[47] the same has its inherent limitations,[48] which include finite sampling and convergence issues, accuracy of the force field, system size, description of the surroundings, etc.

The perturbation of the charged group in a buried pocket is known to overestimate $\Delta\Delta G$ and significantly deviate from the experimental value.[49−51] However, the sign or direction of the calculated $\Delta\Delta G$'s is usually correct. pK_a values of buried ionizable residues (which are related to calculated $\Delta\Delta G$) of nucleases were reported to be significantly overestimated compared to the experiment. Thus, it was proposed that a released proton might remain near the deprotonated residue inside the desolvated pocket. The relatively small pK_a shifts for buried ionizable residues correspond to high apparent dielectric constants in the protein interior. Moreover, (1) water accessibility[52] and conformational relaxation[53] of the ligand binding pocket and (2) absence of explicit electronic polarization (likely the most important factor!!!) in the classical fixed-charge force field may also explain the overestimated relative binding free energy for a charge-changing perturbation in deeply buried pockets.

https://doi.org/10.1021/acsomega.4c10518
ACS Omega 2025, 10, 13966−13976

A sampling of ∼20 μs of MD ensured good convergence of the reported data and a reasonable statistical error (∼1 kcal/mol). Despite the limitations, the present study is valuable for providing (1) a rational approach for substrate-based selective inhibitor design against MtbThyX, (2) a link between atomic interactions and binding affinity, and (3) encouraging experimental investigations. The estimated pK_a of +4.5 units of N3 (dUMP) in the catalytic pocket of MtbThyX from the alchemical binding free energies (dUMP versus $dUMP^{(d)}$ for MtbThyX) agrees with the X-ray structure and previous NMR measurements. However, the experimental binding free energy difference (L1/L2 versus dUMP to thymidylate synthase) is not available, but the reported sign is correct, since the ligands are designed to preferentially bind MtbThyX and strongly disfavored by hThyA, and the magnitude appears to be plausible.

CONCLUSION

In this work, we (1) explored the difference in the substrate binding pocket as well as the nature of the substrate between MtbThyX and hThyA, (2) designed three ligands that were anticipated to be strongly selective in favor of MtbThyX, and (3) evaluated the binding free energy difference (alchemical simulations) of these ligands relative to the substrate (dUMP). We propose L2 and L1 as selective competitive inhibitors of dUMP against MtbThyX, with the former being more promising. Alchemical simulations established a bridge between the relative ligand binding free energy and atomic interactions. The adopted approach could potentially accelerate the discovery of new selective inhibitors against MtbThyX.

ASSOCIATED CONTENT

Data Availability Statement

GROMACS 2022 (https://www.gromacs.org/) was used to carry out simulations and free energy calculations. Hybrid ligand structures and topologies were generated using the open-source PMX package (http://pmx.mpibpc.mpg.de/). ChemDraw 22.2.0 was used to draw 2D structures (https://revvitysignals.com/products/research/chemdraw). The academic version of PyMOL 2 (https://pymol.org/) and VMD 1.9.3 (https://www.ks.uiuc.edu/Research/vmd/) were used for data visualization and trajectory analysis. The input files related to the alchemical simulations are available at https://github.com/pallavsen007/Selective_Inhibitor_ACS_Omega/tree/main.

Supporting Information

The Supporting Information is available free of charge at https://pubs.acs.org/doi/10.1021/acsomega.4c10518.

Alchemical free energy (Tables S1−S3), ADMET properties (Table S4), inter atomic distances (Tables S5 and S6); thermodynamic cycles (Figure S1), probability distribution plots (Figure S2−S4), calculated pK_a (Figure S5), sugar puckering (Figure S6), RMSD (Figures S7 and S8), stacking interaction (Figure S9) (PDF)

AUTHOR INFORMATION

Corresponding Author

Priyadarshi Satpati − *Department of Biosciences and Bioengineering, Indian Institute of Technology Guwahati, Guwahati, Assam 781039, India;* orcid.org/0000-0002-0391-3580; Phone: +91-361-2583205; Email: psatpati@iitg.ac.in; Fax: +91-361-2582249

Author

Pallav Sengupta − *Department of Biosciences and Bioengineering, Indian Institute of Technology Guwahati, Guwahati, Assam 781039, India*

Complete contact information is available at: https://pubs.acs.org/10.1021/acsomega.4c10518

Notes

The authors declare no competing financial interest.

ACKNOWLEDGMENTS

P.S. is thankful to the Ministry of Education (MOE), Govt. of India, for funding. PARAM-ISHAN and PARAM-KAMRUPA at IIT Guwahati are also gratefully acknowledged for providing the computing facility. P.S. acknowledges SERB, Govt. of India (YSS/2015/000024) for funding.

REFERENCES

(1) Myllykallio, H.; Sournia, P.; Heliou, A.; Liebl, U. Unique Features and Anti-Microbial Targeting of Folate- and Flavin-Dependent Methyltransferases Required for Accurate Maintenance of Genetic Information. *Front. Microbiol.* **2018**, *9*, 918.

(2) Myllykallio, H.; Lipowski, G.; Leduc, D.; Filee, J.; Forterre, P.; Liebl, U. An Alternative Flavin-Dependent Mechanism for Thymidylate Synthesis. *Science* **2002**, *297* (5578), 105−107.

(3) Curtin, N. J.; Harris, A. L.; Aherne, G. W. Mechanism of Cell Death Following Thymidylate Synthase Inhibition: 2′-Deoxyuridine-5′-Triphosphate Accumulation, DNA Damage, and Growth Inhibition Following Exposure to CB3717 and Dipyridamole. *Cancer Res.* **1991**, *51* (9), 2346−52.

(4) Ingraham, H. A.; Dickey, L.; Goulian, M. DNA Fragmentation and Cytotoxicity from Increased Cellular Deoxyuridylatet. *Biochemistry* **1986**, *25* (11), 3225−3230.

(5) Chen, D.; Jansson, A.; Sim, D.; Larsson, A.; Nordlund, P. Structural Analyses of Human Thymidylate Synthase Reveal a Site That May Control Conformational Switching between Active and Inactive States. *J. Biol. Chem.* **2017**, *292* (32), 13449−13458.

(6) Baugh, L.; Phan, I.; Begley, D. W.; Clifton, M. C.; Armour, B.; Dranow, D. M.; Taylor, B. M.; Muruthi, M. M.; Abendroth, J.; Fairman, J. W.; Fox, D.; Dieterich, S. H.; Staker, B. L.; Gardberg, A. S.; Choi, R.; Hewitt, S. N.; Napuli, A. J.; Myers, J.; Barrett, L. K.; Zhang, Y.; Ferrell, M.; Mundt, E.; Thompkins, K.; Tran, N.; Lyons-Abbott, S.; Abramov, A.; Sekar, A.; Serbzhinskiy, D.; Lorimer, D.; Buchko, G. W.; Stacy, R.; Stewart, L. J.; Edwards, T. E.; Van Voorhis, W. C.; Myler, P. J. Increasing the Structural Coverage of Tuberculosis Drug Targets. *Tuberculosis* **2015**, *95* (2), 142−148.

(7) Sampathkumar, P.; Turley, S.; Ulmer, J. E.; Rhie, H. G.; Sibley, C. H.; Hol, W. G. J. Structure of the Mycobacterium Tuberculosis Flavin Dependent Thymidylate Synthase (MtbThyX) at 2.0 Å Resolution. *J. Mol. Biol.* **2005**, *352* (5), 1091−1104.

(8) Montfort, W. R.; Perry, K. M.; Fauman, E. B.; Finer-Moore, J. S.; Maley, G. F.; Hardy, L.; Maley, F.; Stroud, R. M. Structure Multiple Site Binding, and Segmental Accommodation in Thymidylate Synthase on Binding dUMP and an Anti-Folate. *Biochemistry* **1990**, *29* (30), 6964−6977.

(9) Koehn, E. M.; Fleischmann, T.; Conrad, J. A.; Palfey, B. A.; Lesley, S. A.; Mathews, I. I.; Kohen, A. An Unusual Mechanism of Thymidylate Biosynthesis in Organisms Containing the ThyX Gene. *Nature* **2009**, *458* (7240), 919−923.

(10) Stull, F. W.; Bernard, S. M.; Sapra, A.; Smith, J. L.; Zuiderweg, E. R. P.; Palfey, B. A. Deprotonations in the Reaction of Flavin-Dependent Thymidylate Synthase. *Biochemistry* **2016**, *55* (23), 3261−3269.

(11) Gaurav, K.; Adhikary, T.; Satpati, P. DUMP/F-DUMP Binding to Thymidylate Synthase: Human Versus Mycobacterium Tuberculosis. *ACS Omega* **2020**, *5* (28), 17182−17192.
(12) Myllykallio, H.; Becker, H. F.; Aleksandrov, A. Mechanism of Naphthoquinone Selectivity of Thymidylate Synthase ThyX. *Biophys. J.* **2020**, *119* (12), 2508−2516.
(13) Koehn, E. M.; Perissinotti, L. L.; Moghram, S.; Prabhakar, A.; Lesley, S. A.; Mathews, I. I.; Kohen, A. Folate Binding Site of Flavin-Dependent Thymidylate Synthase. *Proc. Natl. Acad. Sci. U. S. A.* **2012**, *109* (39), 15722−15727.
(14) Sassetti, C. M.; Rubin, E. J. Genetic Requirements for Mycobacterial Survival during Infection. *Proc. Natl. Acad. Sci. U. S. A.* **2003**, *100* (22), 12989−12994.
(15) Sassetti, C. M.; Boyd, D. H.; Rubin, E. J. Genes Required for Mycobacterial Growth Defined by High Density Mutagenesis. *Mol. Microbiol.* **2003**, *48* (1), 77−84.
(16) Abu El Asrar, R.; Margamuljana, L.; Klaassen, H.; Nijs, M.; Marchand, A.; Chaltin, P.; Myllykallio, H.; Becker, H. F.; De Jonghe, S.; Herdewijn, P.; Lescrinier, E. Discovery of a New Mycobacterium Tuberculosis Thymidylate Synthase X Inhibitor with a Unique Inhibition Profile. *Biochem. Pharmacol.* **2017**, *135*, 69−78.
(17) Kögler, M.; Busson, R.; De Jonghe, S.; Rozenski, J.; Van Belle, K.; Louat, T.; Munier-Lehmann, H.; Herdewijn, P. Synthesis and Evaluation of 6-Aza-2′-Deoxyuridine Monophosphate Analogs as Inhibitors of Thymidylate Synthases, and as Substrates or Inhibitors of Thymidine Monophosphate Kinase in Mycobacterium Tuberculosis. *Chem. Biodivers* **2012**, *9* (3), 536−556.
(18) Kögler, M.; Vanderhoydonck, B.; De Jonghe, S.; Rozenski, J.; Van Belle, K.; Herman, J.; Louat, T.; Parchina, A.; Sibley, C.; Lescrinier, E.; Herdewijn, P. Synthesis and Evaluation of 5-Substituted 2′-Deoxyuridine Monophosphate Analogues as Inhibitors of Flavin-Dependent Thymidylate Synthase in Mycobacterium Tuberculosis. *J. Med. Chem.* **2011**, *54* (13), 4847−4862.
(19) Basta, T.; Boum, Y.; Briffotaux, J.; Becker, H. F.; Lamarre-Jouenne, I.; Lambry, J. C.; Skouloubris, S.; Liebl, U.; Graille, M.; Van Tilbeurgh, H.; Myllykallio, H. Mechanistic and Structural Basis for Inhibition of Thymidylate Synthase ThyX. *Open Biol.* **2012**, *2* (OCT), 120120.
(20) Esra Önen, F.; Boum, Y.; Jacquement, C.; Spanedda, M. V.; Jaber, N.; Scherman, D.; Myllykallio, H.; Herscovici, J. Design, synthesis and evaluation of potent thymidylate synthase X inhibitors. *Bioorg. Med. Chem. Lett.* **2008**, *18* (12), 3628−3631.
(21) Cohen, S. S.; Flaks, J. G.; Barner, H. D.; Loeb, M. R.; Lichtenstein, J. The Mode Of Action Of 5-Fluorouracil And Its Derivatives*. *Proc. Natl. Acad. Sci. U. S. A.* **1958**, *44* (10), 1004−1012.
(22) Parker, W. B.; Cheng, Y. C. Metabolism and Mechanism of Action of 5-Fluorouracil. *Pharmacol. Ther.* **1990**, *48* (3), 381−395.
(23) Hunter, J. H.; Gujjar, R.; Pang, C. K. T.; Rathod, P. K. Kinetics and Ligand-Binding Preferences of Mycobacterium Tuberculosis Thymidylate Synthases, ThyA and ThyX. *PLoS One* **2008**, *3* (5), No. e2237.
(24) Lemos, B. C.; Westphal, R.; Filho, E. V.; Fiorot, R. G.; Carneiro, J. W. M.; Gomes, A. C. C.; Guimarães, C. J.; de Oliveira, F. C. E.; Costa, P. M. S.; Pessoa, C.; Greco, S. J. Synthetic Enamine Naphthoquinone Derived from Lawsone as Cytotoxic Agents Assessed by in Vitro and in Silico Evaluations. *Bioorg. Med. Chem. Lett.* **2021**, *53*, 128419.
(25) Darden, T.; York, D.; Pedersen, L. Particle Mesh Ewald: An N·log(N) Method for Ewald Sums in Large Systems. *J. Chem. Phys.* **1993**, *98* (12), 10089−10092.
(26) Bussi, G.; Donadio, D.; Parrinello, M. Canonical Sampling through Velocity Rescaling. *J. Chem. Phys.* **2007**, *126* (1), 014101.
(27) Parrinello, M.; Rahman, A. Polymorphic Transitions in Single Crystals: A New Molecular Dynamics Method. *J. Appl. Phys.* **1981**, *52* (12), 7182−7190.
(28) Nosé, S.; Klein, M. L. Constant Pressure Molecular Dynamics for Molecular Systems. *Mol. Phys.* **1983**, *50* (5), 1055−1076.
(29) Hess, B.; Bekker, H.; Berendsen, H. J. C.; Fraaije, J. G. E. M. LINCS: A Linear Constraint Solver for Molecular Simulations. *J. Comput. Chem.* **1997**, *18* (12), 1463−1472.
(30) Huang, J.; Rauscher, S.; Nawrocki, G.; Ran, T.; Feig, M.; De Groot, B. L.; Grubmüller, H.; MacKerell, A. D. CHARMM36m: An Improved Force Field for Folded and Intrinsically Disordered Proteins. *Nat. Methods* **2017**, *14* (1), 71−73.
(31) Croitoru, A.; Park, S. J.; Kumar, A.; Lee, J.; Im, W.; Mackerell, A. D.; Aleksandrov, A. Additive CHARMM36 Force Field for Nonstandard Amino Acids. *J. Chem. Theory Comput.* **2021**, *17* (6), 3554−3570.
(32) Jorgensen, W. L.; Chandrasekhar, J.; Madura, J. D.; Impey, R. W.; Klein, M. L. Comparison of Simple Potential Functions for Simulating Liquid Water. *J. Chem. Phys.* **1983**, *79* (2), 926−935.
(33) Vanommeslaeghe, K.; MacKerell, A. D. Automation of the CHARMM General Force Field (CGenFF) I: Bond Perception and Atom Typing. *J. Chem. Inf. Model.* **2012**, *52* (12), 3144−3154.
(34) Van Der Spoel, D.; Lindahl, E.; Hess, B.; Groenhof, G.; Mark, A. E.; Berendsen, H. J. C. GROMACS: Fast, Flexible, and Free. *J. Comput. Chem.* **2005**, *26* (16), 1701−1718.
(35) Olsson, M. H. M.; SØndergaard, C. R.; Rostkowski, M.; Jensen, J. H. PROPKA3: Consistent Treatment of Internal and Surface Residues in Empirical p K a Predictions. *J. Chem. Theory Comput.* **2011**, *7* (2), 525−537.
(36) Søndergaard, C. R.; Olsson, M. H. M.; Rostkowski, M.; Jensen, J. H. Improved Treatment of Ligands and Coupling Effects in Empirical Calculation and Rationalization of p K a Values. *J. Chem. Theory Comput.* **2011**, *7* (7), 2284−2295.
(37) Thurlkill, R. L.; Grimsley, G. R.; Scholtz, J. M.; Pace, C. N. PK Values of the Ionizable Groups of Proteins. *Protein Sci.* **2006**, *15* (5), 1214−1218.
(38) Bennett, C. H. Efficient Estimation of Free Energy Differences from Monte Carlo Data. *J. Comput. Phys.* **1976**, *22* (2), 245−268.
(39) Aylward, N. N. Thermodynamic Constants of the Ionisation of the Acid Imino-Group of Uridine 5′-Monophosphate and Poly-Uridylic Acid. *J. Chem. Soc. B* **1967**, *0*, 401−403.
(40) Sayre, P. H.; Finer-Moore, J. S.; Fritz, T. A.; Biermann, D.; Gates, S. B.; MacKellar, W. C.; Patel, V. F.; Stroud, R. M. Multi-Targeted Antifolates Aimed at Avoiding Drug Resistance Form Covalent Closed Inhibitory Complexes with Human and *Escherichia Coli* Thymidylate Synthases. *J. Mol. Biol.* **2001**, *313* (4), 813−829.
(41) Moore, M. A.; Ahmed, F.; Dunlap, R. B. Evidence for the Existence of Covalent Nucleotide-Thymidylate Synthase Complexes, Identification of Site of Attachment, and Enhancement by Folates*. *J. Biol. Chem.* **1986**, *261* (27), 12745−12749.
(42) Pan, X.; Wang, H.; Li, C.; Zhang, J. Z. H.; Ji, C. MolGpka: A Web Server for Small Molecule PKaPrediction Using a Graph-Convolutional Neural Network. *J. Chem. Inf. Model.* **2021**, *61* (7), 3159−3165.
(43) Daina, A.; Michielin, O.; Zoete, V. SwissADME: A Free Web Tool to Evaluate Pharmacokinetics, Drug-Likeness and Medicinal Chemistry Friendliness of Small Molecules. *Sci. Rep.* **2017**, *7* (1), 1−13.
(44) Lipinski, C. A.; Lombardo, F.; Dominy, B. W.; Feeney, P. J. Experimental and Computational Approaches to Estimate Solubility and Permeability in Drug Discovery and Development Settings. *Adv. Drug Delivery Rev.* **2001**, *46* (1−3), 3−26.
(45) Ghose, A. K.; Viswanadhan, V. N.; Wendoloski, J. J. A Knowledge-Based Approach in Designing Combinatorial or Medicinal Chemistry Libraries for Drug Discovery. 1. A Qualitative and Quantitative Characterization of Known Drug Databases. *J. Comb. Chem.* **1999**, *1* (1), 55−68.
(46) Ertl, P.; Schuffenhauer, A. Estimation of Synthetic Accessibility Score of Drug-like Molecules Based on Molecular Complexity and Fragment Contributions. *J. Cheminf.* **2009**, *1* (1), 8.
(47) Ross, G. A.; Lu, C.; Scarabelli, G.; Albanese, S. K.; Houang, E.; Abel, R.; Harder, E. D.; Wang, L. The Maximal and Current Accuracy of Rigorous Protein-Ligand Binding Free Energy Calculations. *Commun. Chem.* **2023**, *6* (1), 1−12.

https://doi.org/10.1021/acsomega.4c10518
ACS Omega 2025, 10, 13966−13976

(48) Mey, A. S. J. S.; Allen, B. K.; Macdonald, H. E. B.; Chodera, J. D.; Hahn, D. F.; Kuhn, M.; Michel, J.; Mobley, D. L.; Naden, L. N.; Prasad, S.; Rizzi, A.; Scheen, J.; Shirts, M. R.; Tresadern, G.; Xu, H. Best Practices for Alchemical Free Energy Calculations [Article v1.0]. *Living J. Comput. Mol. Sci.* **2020**, *2* (1), 18378.
(49) Wu, X.; Brooks, B. R. Hydronium Ions Accompanying Buried Acidic Residues Lead to High Apparent Dielectric Constants in the Interior of Proteins. *J. Phys. Chem. B* **2018**, *122* (23), 6215−6223.
(50) Isom, D. G.; Castañed, C. A.; Cannon, B. R.; García-Moreno, B. Large Shifts in PKa Values of Lysine Residues Buried inside a Protein. *Proc. Natl. Acad. Sci. U. S. A.* **2011**, *108* (13), 5260−5265.
(51) Harms, M. J.; Castañeda, C. A.; Schlessman, J. L.; Sue, G. R.; Isom, D. G.; Cannon, B. R.; García-Moreno, E. B. The PKa Values of Acidic and Basic Residues Buried at the Same Internal Location in a Protein Are Governed by Different Factors. *J. Mol. Biol.* **2009**, *389* (1), 34−47.
(52) Dwyer, J. J.; Gittis, A. G.; Karp, D. A.; Lattman, E. E.; Spencer, D. S.; Stites, W. E.; García-Moreno, E. B. High Apparent Dielectric Constants in the Interior of a Protein Reflect Water Penetration. *Biophys. J.* **2000**, *79* (3), 1610−1620.
(53) Denisov, V. P.; Schlessman, J. L.; Garcia-Moreno, E. B.; Halle, B. Stabilization of Internal Charges in a Protein: Water Penetration or Conformational Change? *Biophys. J.* **2004**, *87* (6), 3982−3994.

https://doi.org/10.1021/acsomega.4c10518
ACS Omega 2025, 10, 13966−13976